

SSTPI-IM Reconfiguration and Diagnostic under OCF Appearance Used in PV System

Mohamed Ali Zdiri*[‡], Badii Bouzidi**, Mohsen Ben Ammar*, Hsan Hadj Abdallah*

* CEM Laboratory, National Engineering School of Sfax, Tunisia

** RELEV Laboratory, National Engineering School of Sfax, Tunisia

(mohamed-ali.zdiri@enis.tn, badii.bouzidi@enis.tn, mohsen.benammar@enis.tn, hsan.hajabdallah@enis.tn)

[‡] Corresponding Author; Mohamed Ali Zdiri, Control & Energy Management Laboratory (CEMLab), University of Sfax, Sfax Engineering School, BP 1173, 3038 Sfax, Tunisia. E-mail: mohamed-ali.zdiri@enis.tn

Received: 18.11.2020 Accepted: 18.12.2020

Abstract- To enhance the conventional inverter reliability used in PV systems, several diagnostic methods have been investigated. These methods are predominantly applied to detect and identify the IGBT related OCF. In this respect, the present paper puts forward a novel normalized-currents and current-slope information based diagnostic method. Indeed, owing to the critical importance accorded to PV systems following the appearance of IGBT's OCF, the present work is designed to advance a direct RFOC controlled SSTPI-IM diagnostic method and reconfiguration strategy effectively applicable in PV system. Accordingly, fault reconfiguration proves to rest on shifting the SSTPI topology to a FSTPI topology using relays and a redundant leg. The latter is exclusively applicable in case of emerging IGBT fault prevailing in more than a single SSTPI leg. The proposed SSTPI-IM diagnostic method and reconfiguration strategy associated effectiveness and performance, in terms of system continuity as well as fast detection and reconfiguration, are validated through simulation results.

Keywords PV system, Diagnostic methods, IGBT's OCF, SSTPI-IM, Reconfiguration strategy.

Nomenclature

SSTPI: Six switch three-phase inverter
OCF: Open-circuit fault
PV: Photovoltaic
IGBT's: Insulated gate bipolar transistors
RFOC: Rotor flux oriented control
MPPT: Maximum power point tracking
GPV: Photovoltaic generator
IM: Induction motor
SCF: Short-circuit fault
PWM: Pulse with modulation
VSI: Voltage source inverter
MMC: Modular multilevel converter
SMO: Sliding mode observer
FTC: Fault tolerant control
P&O: Perturb and observe
FDM: Fault detection method
MPP: Maximum power point
NCDF: Non-crossed double fault
CDF: Crossed double fault
 I_a, I_b : Currents in the Clarke vector
 I_{as}, I_{bs}, I_{cs} : IM stator currents

w_s : Stator pulsation

I_{max} : Current maximum amplitude

1. Introduction

Given the diversified applications of several industrial domains, such as renewable energy conversion systems, aeronautics and robotics, the conventional power converting systems turn out to be excessively used. In this respect, the PV system stands as one of the most widely popular renewable energy conversion systems, recording an average annual growth rate of 42 % throughout the period ranging from 2000 to 2015 [1]. It is worth noting, however, that for an effective maximization of energy transfer to the load to be achieved, implementing the most appropriate MPPT techniques seem imposed. In this context, the DC-DC converters prove to stand as best fit for implementing these techniques [2-8]. Given the development in the literature, there are several MPPT techniques are used in PV systems such as P&O, incremental conductance, fuzzy logic, ANFIS, neural network (ANN), SMO and deep learning [9-12]. Regarding the present work, however, the examined PV system, subject of study, appears to involve a GPV enclosing

several PV-boost converter modules (modular distribution), a DC-AC converter as well as an IM. Still, given the PV system related complexity, certain power-converter associated faults seem likely to take place. Actually, the occurrence of such faults might well result in a total shutdown of the PV system operation. For this reason, several diagnostic methods and reconfiguration strategies have been continuously developed in the relevant literature. In this context, the present work is exclusively focused on investigating the DC-AC converter related faults.

Generally, the switch OCF and SCF related damages constitute the most widely recurrent faults affecting the DC-AC converters. In effect, the switch SCF related fault is more difficult to detect, and most often occurs quickly, that is why the PV system usually incorporates a set of special hardware protection circuits. On the appearance of switch SCF in the DC-AC converter, the IM must be shut down immediately, and repair is required. The relevant protection circuits are presented in [13]. As for the switch OCF, the fault may well be due to a thermal cycling, likely to result in bonding wires uplifting. It is worth highlighting, in this regard, that the switch OCF does not lead to the PV system shutdown, but can engender secondary failures necessitating urgent monitoring. Hence, for the purpose of further improving the PV system's reliability and maintaining its continuity, it is necessarily to detect, identify and avoid such a fault, which actually constitutes the present paper's focus of interest [14, 15]. In 1976, the model-based fault diagnoses used to be implemented by applying the analytical redundancy method [16]. Then, the remarkable progress noticeable in this regard has paved the way for devising a wide range of diagnostic methods applicable in various systems. Worth citing among them is the diagnostic method based on instantaneous frequency and current vector trajectory information, implemented in a PWM-VSI, as figuring in [17]. Moreover, and for the purpose of detecting and locating the multiple OCF in PWM-VSI, the current slope method has been recently improved, as documented in [18].

In the relevant literature, several diagnostic methods dealing with information on the average currents in the *Park's* vector are also available [19-22]. In this respect, a real time and robust diagnostic method useful for detecting and identifying the OCF switches, implemented in sensorless vector control IM drives is investigated in [23]. A fast diagnosis method for detecting and identifying multiple OCF switch and current sensor related faults in VSI-PMSM drives is advanced in [24]. Similarly, a diagnostic method applied in MMC, based on a half-bridge and SMO switching model is introduced in [25]. As for [26], the FFT algorithm is applied for the purpose of detecting OCF switches in converters. Based on instant voltage error, the OCF switches can be detected and identified using a real-time diagnostic method as illustrated in [27]. Furthermore, a single switch OCF diagnostic method and tolerant control in MMC is introduced in [28].

Among the initially advanced diagnostic methods, some were designed to detect and identify the single switch OCF, while some others were devoted to detecting and identifying the multiple switch OCF. An important step in detecting and

identifying multiple switch OCF, however, is the fault isolation. In addition, developing highly effective reconfiguration strategies to maintain system continuity has drawn a great deal of interest in the relevant literature. For instance, a redundant-leg based FTC has been implemented to highlight the system's reliability under fault compensation condition, as addressed in [29]. Concerning the present paper, however, a fast diagnostic method proposed in [30] is applied to the PV system whereby multiple switch OCF can be rather effectively detected and identified. In effect, the suggested design enables to maintain greater simplicity, robustness against false alarms and low-cost implementation. For the sake of further enhancing the system's reliability and maintaining continuity during an OCF occurrence, a special reconfiguration strategy has been set up. The proposed strategy depends on the switch OCF type, whether single or multiple. In the case of a single and phase OCF, fault reconfiguration is implemented by shifting the topology from SSTPI to FSTPI. As for the others multiple OCF case, however, a redundant leg is provided to maintain fault compensation.

Finally, it is worth noting that the suggested diagnostic method and reconfiguration strategies have proved to help in ameliorating the PV system's reliability and continuity, as the IGBT related OCF can be successfully located, isolated and compensated.

2. PV system description

The studied PV system is structured as in Fig.1.

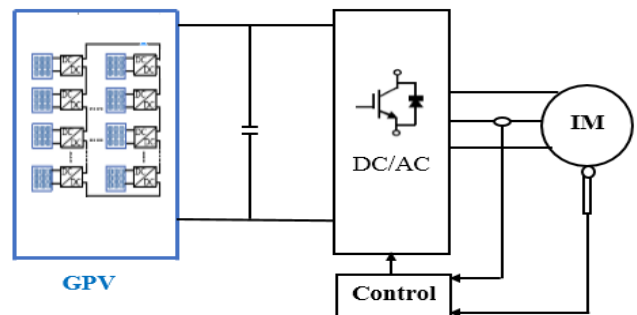


Fig. 1. Diagram of the studied PV system.

Overall, the system's architecture encloses a GPV involving several PV-boost modules (modular distribution), a DC/AC converter as well as an IM. For an effective optimization of the power transfer process to be achieved, we consider implementing a P&O type of MPPT control. The P&O command is the most widely applied technique used in a wide range of photovoltaic applications, owing mainly to its easy and practical implementation [31]. The principle of P&O rests mainly on the duty cycle associated disturbance, as illustrated through Fig.2. To maintain the IM speed performance, the RFOC strategy has been applied in the association of SSTPI-IM. The RFOC implementation scheme is depicted in Fig.3.

3. The investigated diagnostic method

The investigated diagnostic method appears in Fig.4 [30, 32]. Actually, this diagnostic method proves to exhibit a

high-level performance and accuracy against false alarms, enabling to locate and identify the OCF switches in joint association of SSTPI-IM. Accordingly, 27 distinct switch fault signatures can be identified through this investigated diagnostic method, classifiable into five faulty switch conditions, specifically, (a): a single IGBT OCF; (b): a single phase OCF; (c): a NCDF in two different legs; (d): a CDF in two different legs; and (e): three IGBTs' OCF.

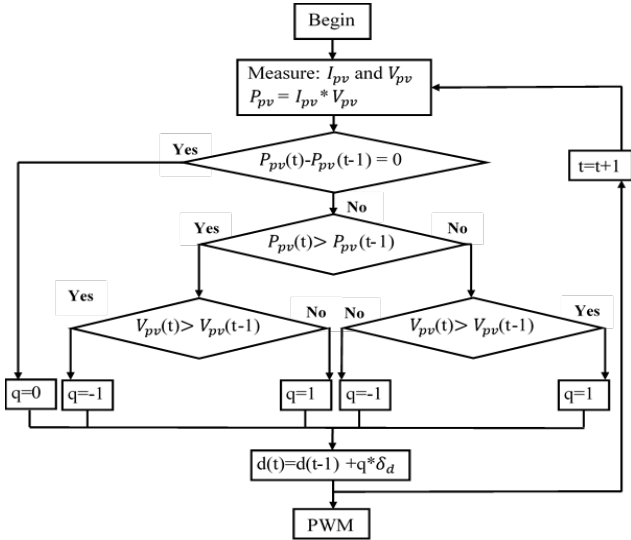


Fig. 2. A flowchart of the P&O type MPPT control.

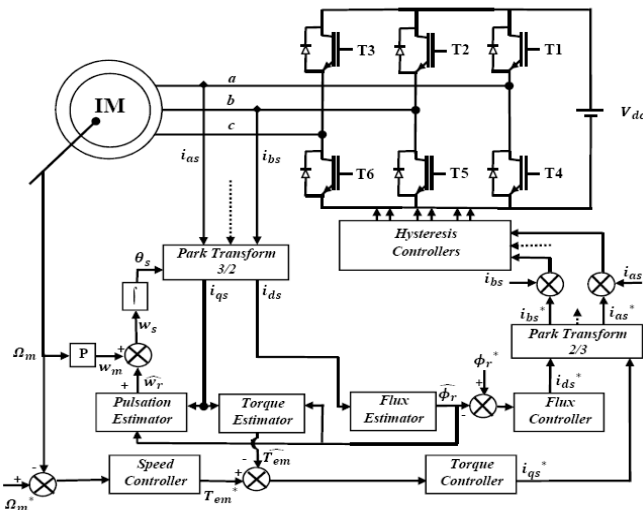


Fig. 3. Diagram of the direct RFOC strategy jointly associated with SSTPI-IM.

This method, subject of investigation, relies essentially on the measurement currents' drawn information, thereby, sparing the need for any additional hardware or extra sensors, and reducing the PV system related cost and complexity. In a first step, relevant information, derived from normalized currents, is drawn by means of the *Clarke* vector modulus. Accordingly, the *Clarke* vector transformation is given by:

$$I_{\alpha} = \sqrt{\frac{3}{2}} I_{as} \quad (1)$$

$$I_{\beta} = \frac{1}{\sqrt{2}} I_{as} + \sqrt{2} I_{bs} \quad (2)$$

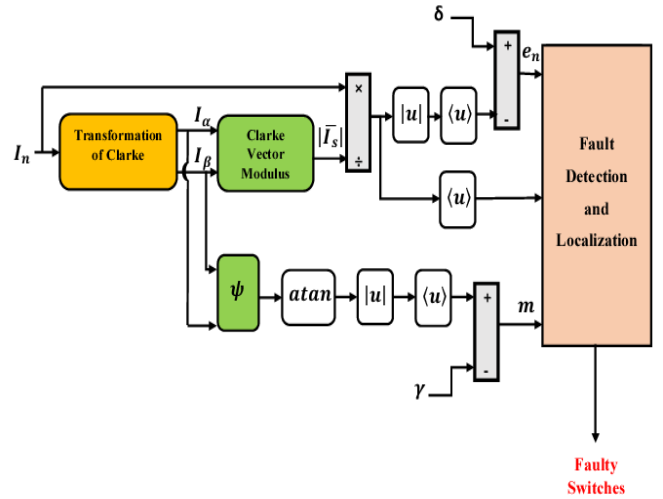


Fig. 4. Diagram of the advanced diagnostic method.

Then, the *Clarke* vector modulus is provided by the following equation:

$$|I_s| = \sqrt{I_{\alpha}^2 + I_{\beta}^2} \quad (3)$$

Hence, the normalized stator currents can be attained by dividing each stator current's phase by the *Clarke* vector modulus, as given by:

$$I_{nN} = \frac{I_n}{|I_s|} \quad (4)$$

Where: $n = as, bs$ and cs .

Throughout the healthy state, the IM stator currents are fluently sinusoidal, as specified by:

$$I_n = \begin{cases} I_{as} = I_{\max} \sin(\omega_s t) \\ I_{bs} = I_{\max} \sin(\omega_s t - \frac{2\pi}{3}) \\ I_{cs} = I_{\max} \sin(\omega_s t + \frac{2\pi}{3}) \end{cases} \quad (5)$$

Overall, the *Clarke* vector modulus is determined through the following equation:

$$|I_s| = \sqrt{\frac{3}{2}} I_{\max} \quad (6)$$

Ultimately, the normalized stator currents can be depicted as follows:

$$I_{nN} = \begin{cases} I_{asN} = \sqrt{\frac{2}{3}} \sin(\omega_s t) \\ I_{bsN} = \sqrt{\frac{2}{3}} \sin(\omega_s t - \frac{2\pi}{3}) \\ I_{csN} = \sqrt{\frac{2}{3}} \sin(\omega_s t + \frac{2\pi}{3}) \end{cases} \quad (7)$$

Relying on the final equation (7), one may well note that the normalized stator currents' associated values do not appear to depend on the stator currents' measured amplitude, comprised within the $\pm\sqrt{\frac{2}{3}}$ range. Accordingly, the average absolute values of the normalized stator currents can be provided by means of:

$$\langle |I_{nN}| \rangle = w_s \int_0^{\frac{1}{w_s}} |I_{nN}| dw_s t \quad (8)$$

The diagnostic method, subject of investigation, rests on the normalized stator currents' average error values, determined through:

$$e_n = \delta - \langle |I_{nN}| \rangle \quad (9)$$

Where: δ defines the normalized stator currents' mean absolute value relevant to the healthy operating conditions, as depicted through:

$$\delta = \frac{1}{\pi} \sqrt{\frac{8}{3}} \approx 0.5198 \quad (10)$$

The introduced error terms e_n are exclusively used to detect and identify the faulty SSTPI legs. Therefore, for the OCF diagnoses of the other types of faults to be achieved, the joint association of the e_n and $\langle |I_{nN}| \rangle$ provided information need be effectively maintained. For the purpose of further enhancing the advanced scheme's performance and robustness against false alarms, a diagnostic error term 'm' has been introduced into the other fault types' diagnoses drawn information.

The error term m depends highly on the current slope associated information, as defined by:

$$\psi = \frac{I_{\alpha k1}}{I_{\beta k1}} \quad (11)$$

Where: $k1$ designates the present sample.

Additionally, the Clarke trajectory related deviation angle ϕ is provided by:

$$\phi = \tan^{-1}(\psi) \quad (12)$$

During healthy operating conditions, the ϕ average absolute value is determined by:

$$\langle |\phi| \rangle = w_s \int_0^{\frac{1}{w_s}} |\phi| dw_s t \quad (13)$$

Hence, the m diagnosis variable is depicted through the following expression:

$$m = \langle |\phi| \rangle - \gamma \quad (14)$$

Where: γ is equal to 0.785 correspondence to the $\langle |\phi| \rangle$ in the healthy case.

Throughout the healthy operating conditions, the entirety of the diagnoses' variables will take values approaching zero. In the OCF case, however, these errors' signatures will be changed to account for the localization and number of faulty IGBTs. Thus, the advanced PV architecture, simultaneously involving the association of SSTPI-IM, as depicted in Fig.5, below:

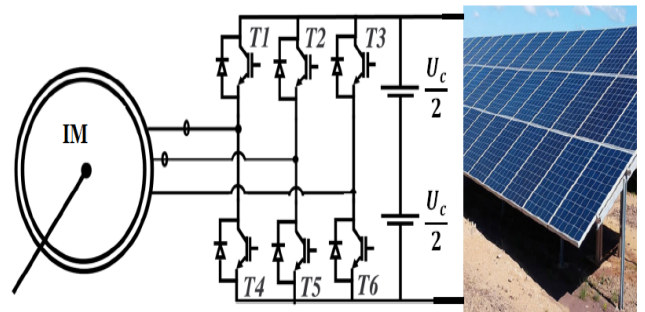


Fig. 5. The SSTPI-IM joint association architecture as used in the PV system.

The investigated diagnostic method is constructed upon analysis of the diagnosis variables associated behaviors relevant to both of the healthy and faulty conditions.

In sum, the advanced framework related diagnosis variables are defined as follows:

$$E_n = \begin{cases} N & \text{for } e_n < 0 \\ 0 & \text{for } 0 \leq e_n < k_f \\ P & \text{for } k_f \leq e_n < k_d \\ D & \text{for } e_n \geq k_d \end{cases} \quad (15)$$

$$S_n = \begin{cases} LL & \text{for } \langle |I_{nN}| \rangle \leq -k_s \\ L & \text{for } -k_s < \langle |I_{nN}| \rangle \\ H & \text{for } 0 < \langle |I_{nN}| \rangle < k_s \\ HH & \text{for } \langle |I_{nN}| \rangle \geq k_s \end{cases} \quad (16)$$

$$M = \begin{cases} SS & \text{for } m \leq k_p \\ S & \text{for } k_p < m < 0 \\ B & \text{for } 0 < m < k_g \\ BB & \text{for } m \geq k_g \end{cases} \quad (17)$$

The entirety of the diagnoses' variables turn out to help in detecting and identifying 27 faulty switch cases, as highlighted in [30]. On accounting for the fast switch OCF detection and robustness against false alarms, the threshold values k_f , k_d , k_s , k_p and k_g can be analyzed by means of the diagnosis variables related behaviors, as depicted under both of the healthy and faulty operating conditions.

4. SSTPI-IM reconfiguration strategy under the IGBT’s OCF occurrence

In a bid to isolate and compensate the IGBT’s OCF, we consider putting forward a new reconfiguration strategy under single and multiple OCF. This reconfiguration strategy rests on using relays (or ideal switch in the simulation) as well as a redundant leg. Actually, the implementing such a strategy is easy, less costly and highly effective.

In the OCF case of a single IGBT or phase, the reconfiguration strategy is ensured by changing the structure of the SSTPI to a FSTPI, without using any redundant leg. Furthermore, Fig.6 highlights well the reconfiguration procedure with respect to the third phase OCF case.

With reference to Fig.6, the relay “RD” undertakes to ensure the removal of the faulty phase, while the relay “RR” serves to maintain the PV system’s continuity by connecting the faulty phase to the DC middle point. At this level, it is worth underlining that in the healthy condition, the relay RD is activated while the relay RR is deactivated. Concerning the other OCF cases, the reconfiguration strategy is maintained by incorporating a redundant leg (T7, T8) in the SSTPI original topology. This new reconfiguration strategy relies on substituting the SSTPI topology with a FSTPI topology, without system shutdown, by adding a redundant leg. The reconfiguration strategy relevant to the case of an OCF appearance in more than a single SSTPI leg is shown in Fig.7. One can well confirm that, following a fault detection via the proposed FDM, the relay RD is deactivated while the relay RR is activated to maintain the PV system’s continuity.

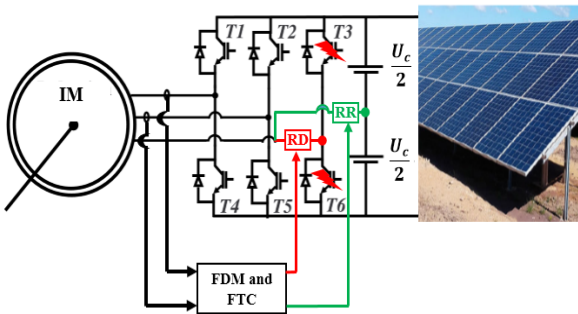


Fig. 6. The reconfiguration strategy scheme under single or phase OCF.

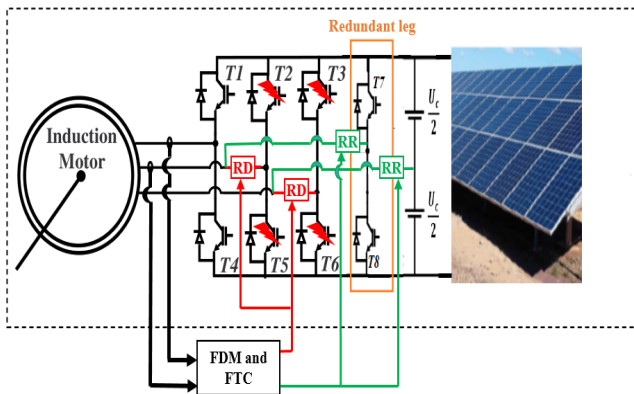


Fig. 7. The reconfiguration strategy scheme under multiple OCF.

5. Simulation results

This section is devoted to discussing and presenting the entire photovoltaic production chain relevant simulations, observed under both of the healthy and faulty operating conditions, on considering the SSTPI-IM association. As simulation subjects, the PV module, boost converter and IM exhibit the following characteristics and parameters, depicted on Tables 1, 2 and 3, below.

Table 1. PV module parameters.

Description	Value
P_{max} (Maximum power in W)	300
V_{mpp} (Voltage at MPP in V)	31.9
I_{mpp} (Current at MPP in A)	9.4
I_{cc} (Short-circuit current in A)	9.75
V_{co} (Open-circuit voltage in V)	39.8

Table 2. Boost converter parameters.

Description	Value
C_e (Input capacity in μF)	0.9804
L (Inductance in mH)	6.8
F (Switching frequency in kHz)	20
C_s (Output capacity in μF)	94.295
Sampling time (sec)	1×10^{-6}

Table 3. IM parameters.

Description	Value
Rated power (kW)	1.1
Rated line voltage (V)	600
Rated speed (rpm)	2820
Rated load torque (N.m)	3.5
Number of pole pairs	1
Stator resistance (Ω)	6.863
Rotor resistance (Ω)	7.67
Stator inductance (H)	0.708
Rotor inductance (H)	0.708
Mutual inductance (H)	0.684
Moment of inertia ($kg.m^2$)	0.0033
Friction factor (N.m.s/rad)	0.00351

5.1. Under healthy condition

Considering the healthy conditions, Fig.8 highlights the PV module (300 W) respective power and current characteristics in voltage terms, with solar irradiation consideration of about 1000 W/m² and a constant temperature of 25 °C. In a bid to optimize the power transfer, a P&O command is used to control the boost converter.

The signature of the boost output voltage concerning each PV module (300 W) along with the signature of the GPV output voltage are shown in Fig.9. Accordingly, one can well notice that each single module associated boost output voltage is equal to 85.13 V. The GPV encloses seven PV modules (of 300 W), with each module incorporating a boost converter (modular structure). In effect, the GPV associated output voltage is roughly equal to 600 V. After the application of the RFOC command in the SSTPI-IM association, Fig.10 outlines the simulations relating to the stator currents, the speed, the torque and the flux, as measured and estimated by their respective references.

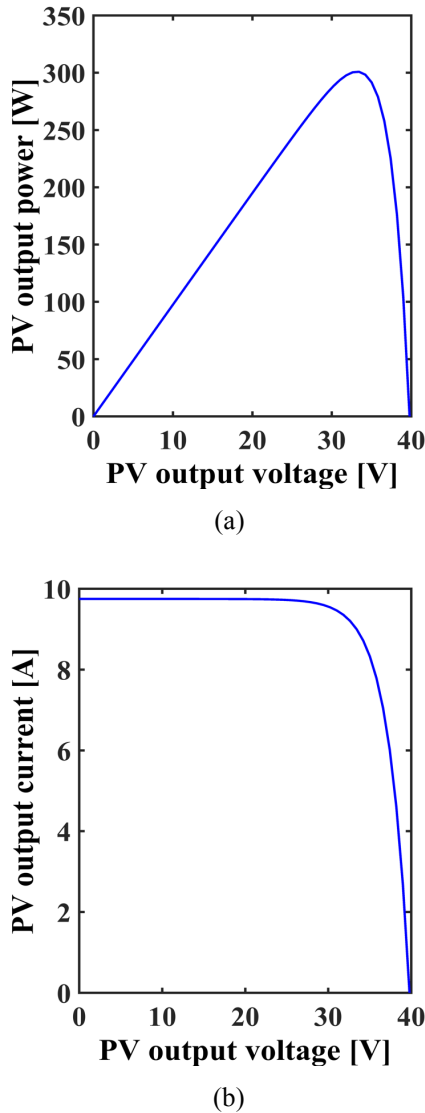


Fig. 8. The PV module relevant characteristics.

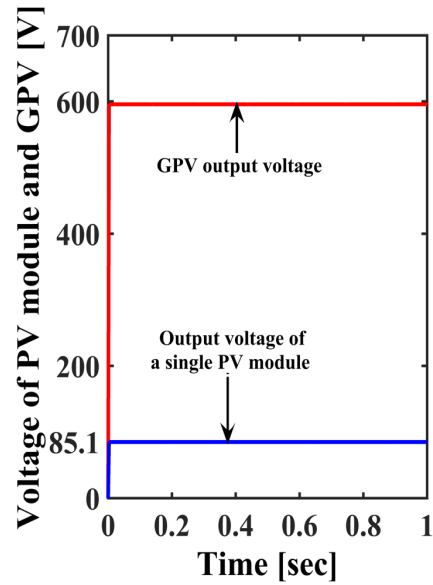


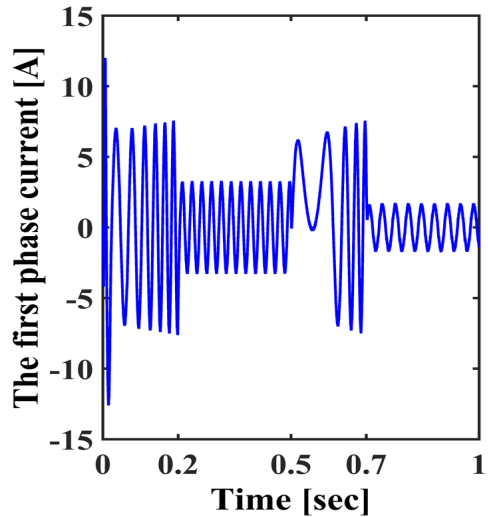
Fig. 9. The output voltage of a single PV module (300 W) and GPV.

The simulation results are depicted through Fig.10, where:

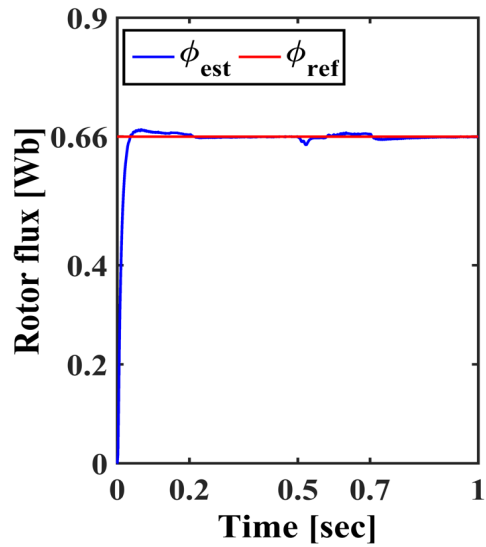
- The stator current shape of the first phase “a” is perfectly sinusoidal, as presented in Fig.10-a;
- The shape of the measured mechanical speed follows its reference speed, displaying an effective dynamic performance, as illustrated in Fig.10-b;
- The shape of the estimated electromagnetic torque along with its respective reference are shown in Fig.10-c. At constant speed, these electromagnetic torques are constant, highlighting the strong dynamic performance of the control; and
- The shape of the estimated rotor flux with its set point are presented in Fig.10-d. The estimated rotor flux appears to follow its set point, characterized with a fluctuation at a reversed motor direction (the magnetization phenomenon).

With respect to the suggested diagnostic method and reconfiguration strategy, the load torque is roughly equal to 1.75 N.m, with a reference speed of about 200 rad/sec. The values associated with the thresholds k_f , k_d , k_s , k_p and k_g are equal to 0.06, 0.275, 0.28, -0.408 and 0.161, respectively [30]. Besides, the IGBT OCF is achieved by removing their gate signal with the anti-parallel diode connected.

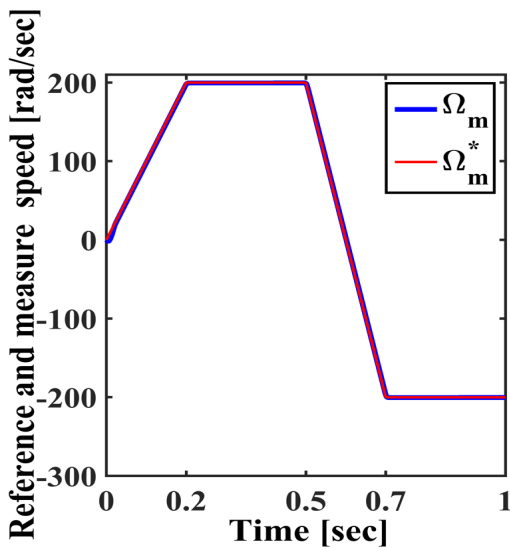
As for the following section, it is devoted to observing the faulty case. It is worth underlining, in this context, that, the investigated reconfiguration strategy is applied when the IGBT’s OCF’s are detected and identified through the diagnostic method advanced.



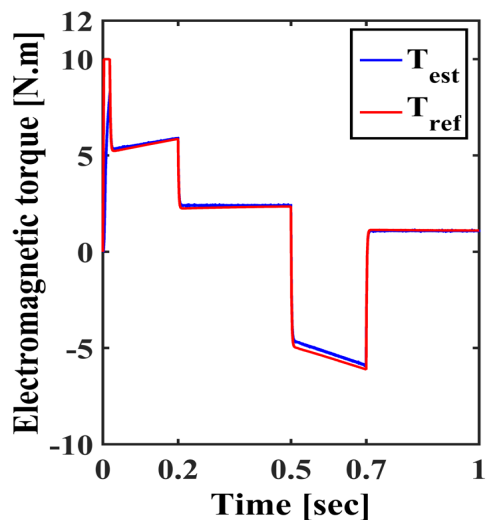
(a)



(d)



(b)



(c)

Fig. 10. The Speed control via direct RFOC command from the IM, powered by a SSTPI. **Legend:** (a): stator current of the first phase “a”, (b): measured speed (Ω_m) and reference speed (Ω_m^*), (c): estimated torque and its reference, and (d): estimated flux and its reference.

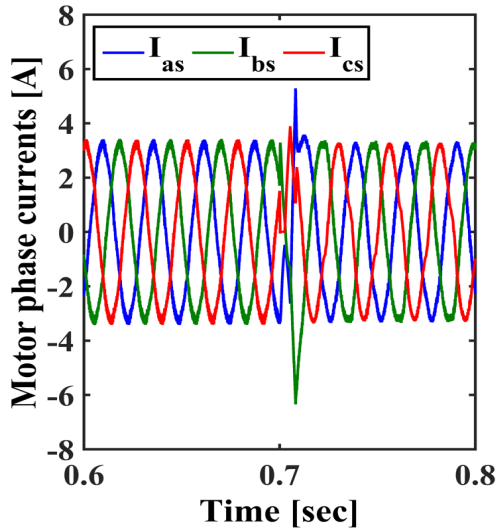
5.2. Under a faulty case

5.2.1 Single or phase OCF

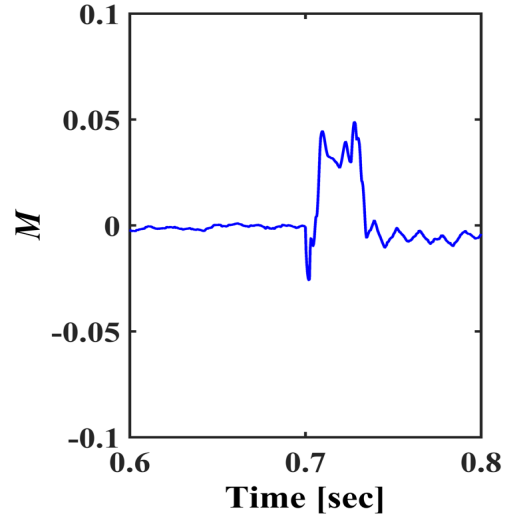
The IM stator currents together with E_n , S_n and M are presented in Fig.11. The OCF of IGBT T3 is undertaken at time $T = 0.7$ sec. Actually, the OCF is detected and identified via the advanced diagnostic method at time $T = 0.7027$ sec, corresponding to the intersection of E_{cs} with k_f . Hence, to compensate the OCF and maintain the PV system’s continuity, the reconfiguration strategy must be applied.

Thus, the reconfiguration strategy relevant to the OCF case is achieved by removing the faulty SSTPI leg and connecting the faulty IM phase to the DC middle point. With reference to Fig.11, one can well confirm that the OCF compensation is reached when the E_n turn out to approach the zero value, which corresponds to the instant $T = 0.7352$ sec. At this time level, the behaviors associated with the other diagnosis variables are similar.

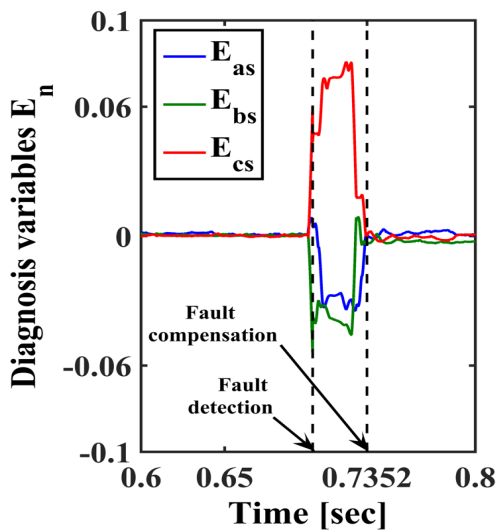
In sum, the proposed diagnostic method and reconfiguration strategy prove to require just 0.0027 sec and 0.0325 sec, respectively, in order to detect, identify and compensate the T3 IGBT OCF. This reconfiguration strategy remains the same with respect to the third phase OCF case. It is worth highlighting that this reconfiguration strategy does not require any redundant leg.



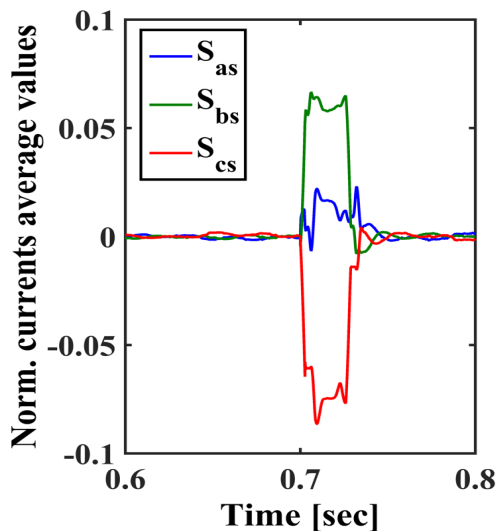
(a)



(d)



(b)



(c)

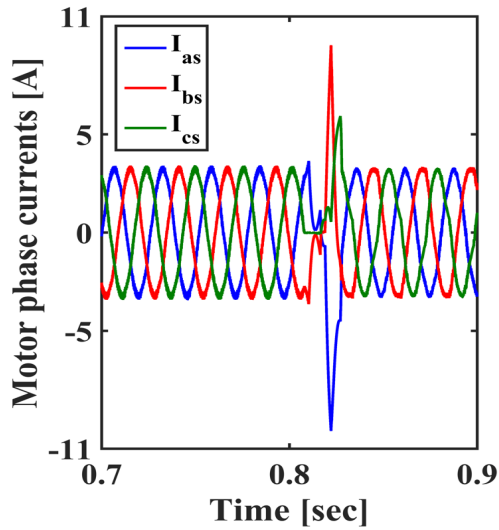
Fig. 11. Simulation results considering the healthy case, faulty case (IGBT T3) and compensation case. **Legend:** (a): IM stator currents; (b): E_n ; (c): S_n , and (d): M .

5.2.1 The remaining IGBT's OCF cases

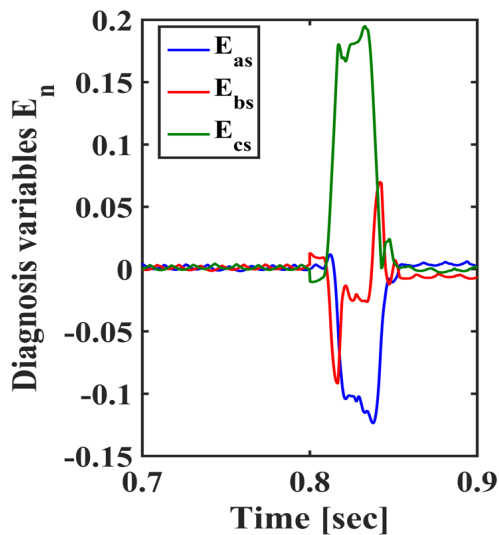
It is worth noting that in these faulty cases, the reconfiguration strategy does not appear to be similar to the first faulty case (single or phase OCF). The IM stator currents along with E_n , S_n and M , for a double OCF in the IGBTs T2 and T6 (the second and third phases' faults), are shown in Fig.12. These IGBTs related OCFs are achieved at the instant $T = 0.8$ sec.

Noteworthy, also, is that when the diagnosis variable M attains the value 0.1, corresponding to the instant $T = 0.8174$ sec, the IGBTs' OCFs are detected and identified via the proposed diagnostic method. Accordingly, to compensate these faults and maintain the PV system's continuity, the reconfiguration process is undertaken by inserting a redundant leg. More specifically, the redundant leg (T7, T8) maintaining the same command would substitute the second SSTPI leg (T2, T5), and the third SSTPI leg is removed. In addition, the DC middle point undertakes to connect the third IM faulty phase. It is worth stating that in the OCFs cases, the SSTPI topology is usually substituted with the FSTPI topology to maintain the PV system's continuity. Regarding Fig.12, one could well note that the fault compensation procedure is achieved at the moment when M is almost equal to zero, which corresponds to the instant $T = 0.8472$ sec. At this time level, the entirety of the diagnosis variables' behaviors are the same.

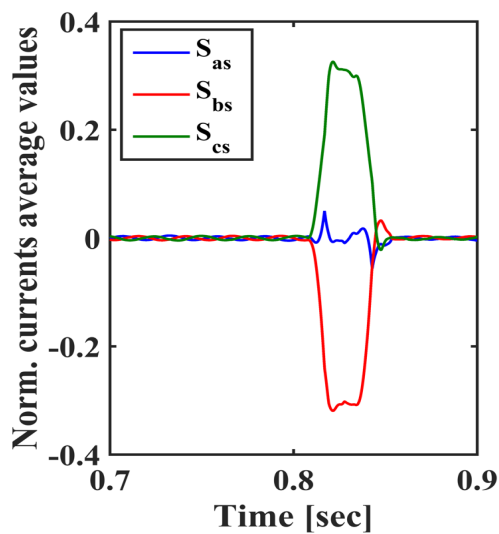
Worth highlighting, in the end, is that the advanced diagnostic method and reconfiguration strategy prove to require just 0.0174 sec and 0.0472 sec, respectively, to detect, identify and compensate the IGBTs' OCFs. This reconfiguration scheme proceeds in the same way with respect to the multiple OCF case, on excluding the single and phase OCF case.



(a)



(b)



(c)

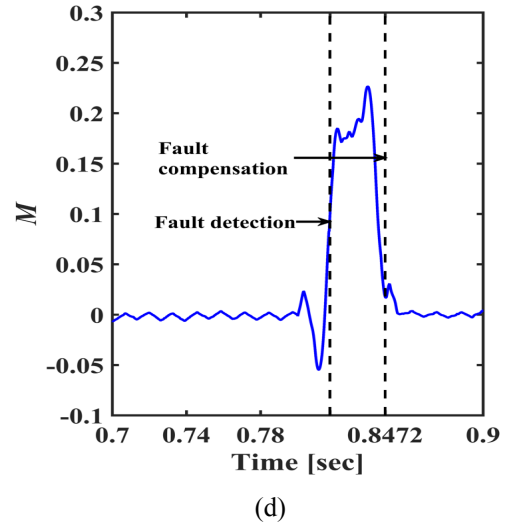


Fig. 12. Simulation results considering the healthy case, faulty case (T2, T6) and compensation case. **Legend:** (a): IM stator currents; (b): E_n ; (c): S_n , and (d): M .

6. Conclusion

In this work, a reconfiguration strategies applied in PV system is put forward. Aimed at compensating single and multiple IGBT OCF, the reconfiguration architecture intervenes, following a fault detection and identification process, by means of a specifically designed FDM. Overall, the advanced diagnostic method proves to display a set of distinctive features, particularly, a prompt OCF detection procedure, low-cost implementation as well as a highly effective robustness against false alarm problems. This diagnostic method relies mainly on information concerning the normalized measured currents and current slope.

As to the fault compensation scheme, it rests basically on shifting the SSTPI topology to a FSTPI topology by means of special relays and a redundant leg. The latter acts exclusively during the fault emergence circumstances affecting more than a single SSTPI leg. The proposed reconfiguration strategies require approximately 0.047 sec in order to maintain the PV system continuity. It is also important to note that, throughout the IGBT's OCF compensation process, no noticeable loss of reliability, power flow and PV system continuous functioning can be perceived.

Ultimately, the simulation results achieved in regard to the designed diagnostic method and reconfiguration strategies turn out to demonstrate high-level performance and efficiency in terms of IGBT's OCFs detection, isolation and compensation.

Acknowledgements

The present work has been funded by the Ministry of Higher Education of Tunisia. We would also like to thank, sincerely, Mr. Sami CHAMI; a Senior University Teacher of English, exercising at the National Engineering School of

Sfax, Tunisia, for his valuable contribution in regard to linguistic proofreading and structural revision of this paper.

References

- [1] I. G. Zurbriggen, and M. Ordonez, "PV Energy Harvesting Under Extremely Fast Changing Irradiance: State-Plane Direct MPPT", *IEEE Trans. Ind. Electron.*, vol. 66, no. 3, pp. 1852-1861, 2019.
- [2] E. Jamshidpour, P. Poure, and S. Saadate, "Common switch fault diagnosis for two-stage DC-DC converters used in energy harvesting applications", *Electronics*, vol. 8, no. 3, pp. 293, 2019.
- [3] F. Blaabjerg, Z. Chen, and S.B. Kjaer, "Power electronics as efficient interface in dispersed power generation systems", *IEEE Trans. Power Electron.*, vol. 19, no. 5, pp. 1184-1194, 2004.
- [4] C. Xu, C. Pan, Y. Liu, and Z.L. Wang, "Hybrid cells for simultaneously harvesting multi-type energies for self-powered micro/nano systems", *Nano Energy*, vol. 1, no. 2, pp. 259-272, 2012.
- [5] A.A. Khan, A. Mahmud, and D.B. Ban, "Evolution From Single To Hybrid Nano generator: A Contemporary Review On Multimode Energy Harvesting For Self-Powered Electronics", *IEEE Trans. Nanotechnol.*, vol.18, pp. 21-36, 2018.
- [6] K. Kumar, S.K. Rafi, R. Tiwari, S. Saravanan, P. Pandiyan, and N. Prabakaran, "Performance Evaluation of Photo Voltaic System with Quadratic Boost Converter Employing with MPPT Control Algorithms", *International Journal of Renewable Energy Research (IJRER)*, vol. 10, no. 3, pp. 1083-1091, 2020.
- [7] M.K. Al-Nussairi, R. Bayindir, and E. Hossain, "Fuzzy logic controller for Dc-Dc buck converter with constant power load", In 2017 IEEE 6th International Conference on Renewable Energy Research and Applications (ICRERA), pp. 1175-1179, 2017.
- [8] K. Kajiwara, N. Matsui, and F. Kurokawa, "A new MPPT control for solar panel under bus voltage fluctuation", In 2017 IEEE 6th International Conference on Renewable Energy Research and Applications (ICRERA), pp. 1047-1050, 2017.
- [9] D. Haji, and G. Naci, "Dynamic Behavior Analysis of ANFIS Based MPPT Controller for Standalone Photovoltaic Systems", *International Journal of Renewable Energy Research (IJRER)*, vol. 10, no. 1, pp. 101-108, 2020.
- [10] E. Kurt, and G. Soykan, "Performance Analysis of DC Grid Connected PV System Under Irradiation and Temperature Variations", In 2019 8th International Conference on Renewable Energy Research and Applications (ICRERA), pp. 702-707, 2019.
- [11] S. Marhraoui, A. Abbou, N. El Hichami, S.E. Rhaili, and M.R. Tur, "Grid-Connected PV Using Sliding Mode Based on Incremental Conductance MPPT and VSC", In 2019 8th International Conference on Renewable Energy Research and Applications (ICRERA), pp. 516-520, 2019.
- [12] A. Ali, A.N. Hasan, and T. Marwala, "Perturb and observe based on fuzzy logic controller maximum power point tracking (MPPT). In 2014 International Conference on Renewable Energy Research and Application (ICRERA), pp. 406-411, 2014.
- [13] B. Lu, and S.K. Sharma, "A literature review of igt fault diagnostic and protection methods for power inverters", *IEEE Trans. on Ind. Appl.*, vol. 45, no. 5, pp. 1770-1777, 2009.
- [14] M.A. Zdiri, B. Bouzidi, and H. Hadj Abdallah, "Reconfiguration strategy of SSTPI to FSTPI after the appearance of a single-IGBT OCF and a single-phase OCF", In: *International Conference on Recent Advances in Electrical Systems, Conferences Publications, Hammamet, Tunisia*, pp. 177-182, 2019.
- [15] D. Xie, J. Pu, and X. Ge, "Current residual-based method for open-circuit fault diagnosis in single-phase PWM converter", *IET Power Electr.*, vol. 11, no. 14, pp. 2279-2285, 2018.
- [16] A.S. Willsky, "A survey of design methods for failure detection in dynamic systems", *Automatica*, vol. 12, no. 6, pp. 601-611, 1976.
- [17] R. Peugot, S. Courtine, and J.P. Rognon, "Fault detection and isolation on a pwm inverter by knowledge-based model", *IEEE Trans. on Ind. Appl.*, vol. 34, no. 6, pp. 1318-1326, 1998.
- [18] M. Trabelsi, M. Boussak, and M. Gossa, "Multiple igtbs open circuit faults diagnosis in voltage source inverter fed induction motor using modified slope method", in *The XIX International Conference on Electrical Machines - ICEM 2010*, pp. 1-6, 2010.
- [19] S.M.A. Cruz, and A.J.M. Cardoso, "Stator winding fault diagnosis in three-phase synchronous and asynchronous motors, by the extended park's vector approach", *IEEE Trans. on Ind. Appl.*, vol. 37, no. 5, pp. 1227-1233, 2001.
- [20] D. Diallo, M.E.H. Benbouzid, D. Hamad, and X. Pierre, "Fault detection and diagnosis in an induction machine drive: A pattern recognition approach based on concordia stator mean current vector", *IEEE Trans. on Energy Conv.*, vol. 20, no. 3, pp. 512-519, 2005.
- [21] J.A.A. Caseiro, A.M.S. Mendes, and A.J.M. Cardoso, "Fault diagnosis on a pwm rectifier ac drive system with fault tolerance using the average current park's vector approach", *IEEE International Electric Machines and Drives Conference*, pp. 695-701, 2009.
- [22] J.O. Estima, N.M.A. Freire, and A.J.M. Cardoso, "Recent advances in fault diagnosis by park's vector approach", *IEEE Workshop on Electrical Machines Design, Control and Diagnosis (WEMDCD)*, pp. 279-288, 2013.
- [23] R. Maamouri, M. Trabelsi, M. Boussak, and F. M'Sahli, "A sliding mode observer for inverter open-

- switch fault diagnostic in sensorless induction motor drive”, in IECON 2016 - 42nd Annual Conference of the IEEE Industrial Electronics Society, pp. 2153-2158, 2016.
- [24] I. Jlassi, J.O. Estima, S.K.E. Khil, N.M. Bellaaj, and A.J.M. Cardoso, “A robust observer-based method for igbts and current sensors fault diagnosis in voltage-source inverters of pmsm drives”, IEEE Trans. on Ind. Appl., vol. 53, no. 3, pp. 2894-2905, 2017.
- [25] S. Shao, P.W. Wheeler, J.C. Clare, and A.J. Watson, “Fault detection for modular multilevel converters based on sliding mode observer”, IEEE Trans. on Power Electr., vol. 28, no. 11, pp. 4867-4872, 2013.
- [26] C. Gan, J. Wu, S. Yang, Y. Hu, W. Cao, and J. Si, “Fault diagnosis scheme for open-circuit faults in switched reluctance motor drives using fast fourier transform algorithm with bus current detection”, IET Power Electr., vol. 9, no. 1, pp. 20-30, 2016.
- [27] L.M.A. Caseiro, and A.M.S. Mendes, “Real-time igbt open-circuit fault diagnosis in three-level neutral-point-clamped voltage-source rectifiers based on instant voltage error”, IEEE Trans. on Ind. Electr., vol. 62, no. 3, pp. 1669-1678, 2015.
- [28] B. Li, S. Shi, B. Wang, G. Wang, W. Wang, and D. Xu, “Fault diagnosis and tolerant control of single igbt open-circuit failure in modular multilevel converters”, IEEE Trans. on Power Electr., vol. 31, no. 4, pp. 3165-3176, 2016.
- [29] R. Maamouri, M. Trabelsi, M. Boussak, and F. M'Sahli, “Fault Diagnosis and Fault Tolerant Control of a Three-Phase VSI Supplying Sensorless Speed Controlled Induction Motor Drive”, Electric Power Comp. and Syst., vol. 46, no. 19-20, pp. 2159-2173, 2018.
- [30] M.A. Zdiri, B. Bouzidi, and H. Hadj Abdallah, “Performance investigation of an advanced diagnostic method for SSTPI-fed IM drives under single and multiple open IGBT faults”, COMPEL International Journal of Computations and Mathematics in Electrical, vol. 38, no. 2, pp. 616-641, 2019.
- [31] N. Femia, G. Petrone, G. Spagnuolo, and M. Vitelli, “A Technique for Improving P&O MPPT Performances of double-stage grid-connected photovoltaic systems”, IEEE Trans. on Indus. Electr., vol. 56, no. 11, pp. 4473-4482, 2009.
- [32] M.A. Zdiri, B. Bouzidi, and H. Hadj Abdallah, Performance investigation of an improved diagnostic method for open IGBT faults in VSI fed IM drives, In Diagnosis, Fault Detection & Tolerant Control, Springer, Singapore, pp. 155-171, 2020.